

# Questioning a 3.5 keV dark matter emission line

Signe Riemer-Sørensen<sup>1,\*</sup>

<sup>1</sup>*Institute of Theoretical Astrophysics, University of Oslo, PO 1029 Blindern, 0315 Oslo, Norway*

Recent results of line emission at 3.5 keV in both individual and stacked X-ray spectra of galaxy clusters has been speculated to have dark matter origin. We analyse *Chandra* X-ray observations of the Milky Way where, if the origin is indeed dark matter, such a line should be very strong. We find no clear evidence for its presence but the results are strongly dependent on the assumptions about the astrophysical sources, that goes into the spectral modelling. For the most conservative assumptions the Milky Way observations are consistent with a line at 3.5 keV but when excluding known emission lines, the allowed extra emission significantly decreases and rules out the predicted line at 95% confidence level. We present flux limits and interpretations for various scenarios (decaying and annihilating dark matter).

## I. INTRODUCTION

Recent results by Bulbul *et al.* [1] and Boyarsky *et al.* [2] show an excess of emission around  $\approx 3.5$  keV in both individual and stacked X-ray spectra of galaxy clusters. The spectral shape is consistent with mono-energetic line emission. There are no obvious astrophysical origins and alternative options such as dark matter has been considered [1–8]. If this is the case, it should also be emitted in the Milky Way providing a nearby consistency check. We analyse stacked X-ray spectra towards the Milky Way Centre to look for such a line but find no clear evidence for its existence.

The analysed data is described in Sec. II and the spectral modelling in Sec. III. In Sec. IV we present a conservative determination of the observed mass within the field of view, before we present general constraints on flux and decay rate for both decaying and annihilating dark matter in Sec. V and more specific constraints on sterile neutrinos in Sec. VI

## II. DATA

We use a number of publicly available<sup>1</sup> *Chandra* X-ray observations of the region within 20 arcmin of Sgr A\* located at (RA, Dec) = (17 h 45 m 40.0409 s, -29° 0' 28.118'') corresponding to galactic coordinates ( $l, b$ ) = (359.944°, -0.04605°). The observation identification numbers (Obs ID) and exposure times are listed in Tab. I. All the selected exposures are observed with the ACIS I0-I3 chips and consequently the total field of view is a square of 16.8 arcmin  $\times$  16.8 arcmin. The raw data were processed chip-by-chip using the software package, CIAO,<sup>2</sup> following the ACIS data analysis guide.<sup>3</sup> In brief the steps are:

Obs ID	Raw exposure [ks]	Cleaned [ks]
3392	167.0	166.0
3393	160.1	157.7
3665	91.1	89.7
5935	46.0	45.1
10556	114.0	112.2
11843	80.0	78.8
13438	67.0	66.0
Total	825.0	750.6

TABLE I. Public *Chandra* observations used in the analysis.

**Reprocessing:** The files are reprocessed to ensure the application of the most up-to-date calibration database (CALDB) and to set the observation specific bad pixel file so cosmic rays etc. are excluded from the analysis. All observations were taken in faint mode, which uses a  $3 \times 3$  pixel island to grade the events for bad pixel exclusion.

**Source region selection:** For each chip we avoid the edges by cutting a square of 8 arcmin  $\times$  8 arcmin. We also exclude a circle with radius of 2.5 arcmin around Sgr A\* as demonstrated in Fig. 1.

**Point source removal and deflaring:** Point sources were removed from the images using the wavdetect routine in CIAO. Likewise we removed periods with flaring activity where the flux exceeded  $\pm 3\sigma$  of the mean.

**Background selection:** We do not remove any background from the observations, but rather add the line emission visible in observations taken with the telescope in the stowed position (“lid on”) to the model later (denoted “instrumental lines” in Tab. II).

**Spectrum extraction:** The spectra were extracted for the source regions described above as well as the instrumental response files necessary to perform the analysis in physical units and to compensate for a non-uniform effective collecting area on the detector.

**Stacking:** The spectra are weighted and stacked using the combine\_spectra routine in CIAO. The resulting stacked spectrum of all four chips is showed in Fig. 2.

\* Email: signe.riemer-sorensen@astro.uio.no

<sup>1</sup> <http://cda.harvard.edu/chaser/>

<sup>2</sup> <http://cxc.harvard.edu/ciao/> version 4.6 with CALDB 4.6.1

<sup>3</sup> <http://cxc.harvard.edu/ciao/guides/>

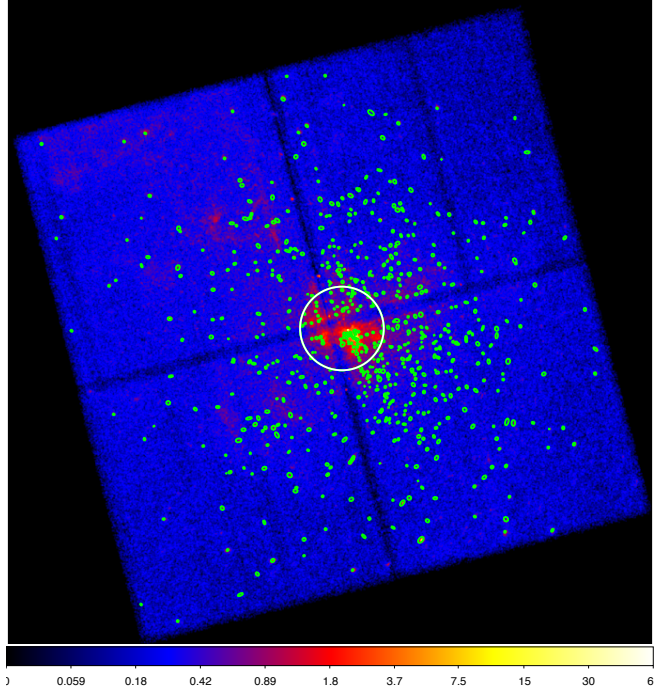


FIG. 1. Example of the raw data of observation 3392 with the regions removed as point sources (small green ellipses) and Sgr A (white circle) highlighted. The data have been smoothed with a 5 pixel Gaussian for visualisation purposes.

### III. SPECTRUM MODELLING

Modelling the astrophysical X-ray emission of the Milky Way centre is notoriously difficult because many sources contribute with a range of different signatures [9] that may hide the line we're looking for. Consequently we explore different assumptions when constraining the allowed excess line emission flux.

The base for our explorations is a line-free apec model [10] combined with a power law and a Gaussian at 9.7 keV to mimic residual detector background. This model is pre-fitted to intervals that appear line-free (2.01–2.2 keV, 5.5–5.6 keV, 8.5–9.0 keV), before we add known instrumental lines and metal emission lines with emissivities larger than  $5 \times 10^{-19}$  photons cm $^{-3}$  sec $^{-1}$  (for a plasma temperature of 2 keV) as listed in Tab. II [same metal lines as in 1]. The central value of the emission lines are allowed to “budge” by 0.01 keV in the fit to account for uncertainties and mis-calibrations in the spectra. The widths are assumed to be unresolved (but we have checked that allowing for broadening up to 0.1 keV does not improve the fit quality). We remove those lines that do not change the best fit  $\chi^2$  (marked in Tab. II). On top of the best fit base model we add an unresolved Gaussian to account for non-astrophysical line emission. For each central energy in 0.05 keV steps, we fit the model to the stacked spectrum, and then increase the normalisation of the additional Gaussian until  $\Delta\chi^2 = \chi^2(\text{norm}) - \chi^2(\text{best fit}) = 4$  corresponding to

the upper 95% confidence level for one degree of freedom (the normalisation). The line flux is calculated in bins of Full Width Half Max (FWHM) of the spectral resolution around the central value approximated by [11]

$$\Delta E_{FWHM} = 0.012E_\gamma + 0.12 \text{ keV}. \quad (1)$$

We consider two energy intervals for the base model fit namely the broad interval of 2.0 – 9.0 keV, and the narrower interval of 3.0 – 6.0 keV. For the base model the best fit  $\chi^2$ 's are 5.2 and 1.7 for the broad and narrow intervals respectively. The major contribution to the  $\chi^2$  of the broad interval comes from the emission line dominated energies below 3 keV. For each energy we then consider two different constraints: a) the entire flux in all Gaussians including metals and instrumental lines, and b) the flux in the additional line only. The former is a very conservative limit as we know some of the line flux can have astrophysical origin, but it takes into account the risk of a non-astrophysical line hiding under an astrophysical emission line. The latter is much less conservative and does not take the “hiding” effect into account but assumes that all line emission at the metal line energies origin from the metals. The resulting flux limits are shown in Fig. 3.

### IV. MASS WITHIN FIELD OF VIEW

The dark matter emission scales with the amount of dark matter within the observed field of view. We calculate the mass within the field of view as the integral along the line of sight within a 16 arcmin $\times$ 16 arcmin square, assuming the density variation over this region to be negligible. We subtract the area of a circle with radius of 2.5 arcmin to account for the removed region around Sgr A\* (8%) and an additional 7% to account for the removed point sources.

For the dark matter density profile as a function of radius ( $r$ ), we conservatively use an Einasto profile [13]

$$\rho_{\text{DM}}(r) = \rho_\odot \exp \left[ -\frac{2}{\alpha} \left( \left( \frac{r}{r_s} \right)^\alpha - \left( \frac{r_\odot}{r_s} \right)^\alpha \right) \right], \quad (2)$$

where  $r_s = 21$  kpc is the scale radius,  $\rho_\odot = 0.4 \text{ GeV kpc}^{-3} = 10.5 \times 10^6 M_\odot \text{ kpc}^{-3}$  is the density at the solar radius  $r_\odot = 8.3$  kpc from the galactic centre, and  $\alpha = 0.17$  [14]. This gives a total mass within the field of view of  $M_{\text{fov}} = 2.8 \times 10^6 M_\odot$  with a mass-weighted average distance of  $D_{\text{avg}} = 8.9$  kpc. For annihilating dark matter or scattering processes, the probability is proportional to the integral over density squared rather than density, leading to  $5.9 \times 10^{15} M_\odot^2 \text{ kpc}^{-3}$  at 8 kpc.

Simulations indicate that the dark matter profiles may be steeper than the Einasto profile. If we instead use a Navarro-Frenk-White (NFW) profile [15]

$$\rho_{\text{DM}}(r) = \rho_\odot \frac{r_\odot \left( 1 + \left( \frac{r_\odot}{r_s} \right) \right)^2}{r \left( 1 + \left( \frac{r}{r_s} \right) \right)^2} \quad (3)$$

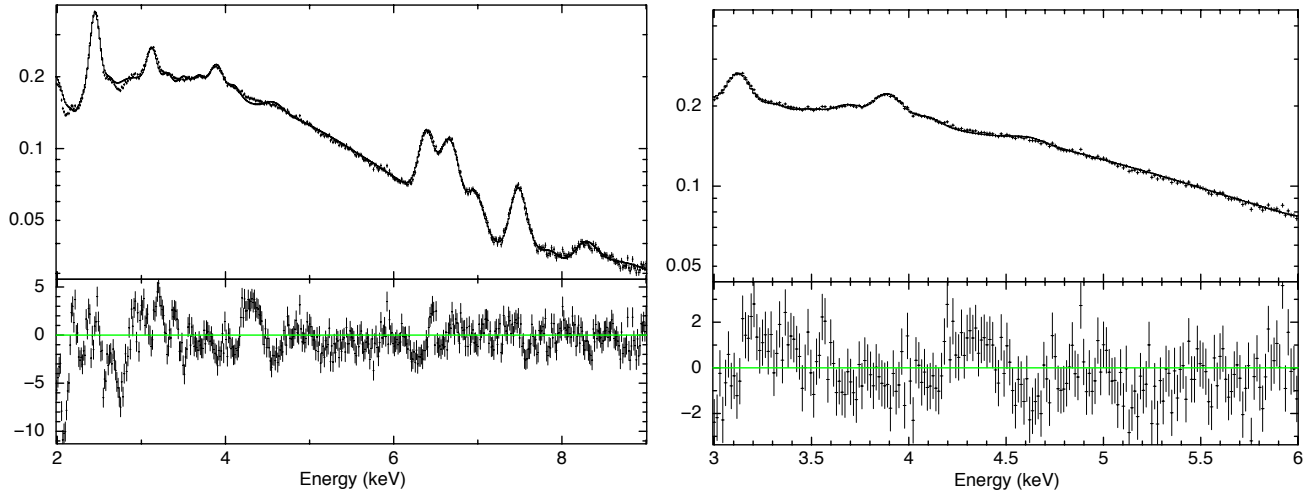


FIG. 2. The stacked spectrum and best-fit model (without any additional line emission) in normalised counts  $\text{keV}^{-1} \text{sec}^{-1}$ , and  $\chi^2$  residuals below for the 2.0 – 9.0 keV (left) and 3.0 – 6.0 keV (right) intervals. No significant emission line excess is seen around 3.5 keV.

Emission lines				Instrumental lines			
Energy [keV]	Line	Energy [keV]	Line	Energy [keV]	Line	Energy [keV]	Line
2.01	Si XIV	3.47 <sup>bc</sup>	K XVIII	6.39 <sup>bc</sup>	Fe K- $\alpha$	1.49	Al K- $\alpha$
2.05	Al XIII	3.51 <sup>bc</sup>	K XVIII	6.70	Fe XXV	1.74	Si K- $\alpha$
2.18 <sup>b</sup>	Si XII	3.62 <sup>bc</sup>	Ar XVII	6.62 <sup>b</sup>	Fe XXIV	2.15 <sup>bc</sup>	Au M- $\alpha\beta$
2.29 <sup>b</sup>	Si XII	3.68 <sup>bc</sup>	Ar XVII	6.95 <sup>b</sup>	Fe XXIV	7.46	Ni K- $\alpha$
2.34 <sup>b</sup>	Si XII	3.71 <sup>bc</sup>	K XIX	7.29 <sup>b</sup>	Fe XXV	9.71 <sup>bc</sup>	Au L- $\alpha$
2.45 <sup>b</sup>	Si XV	3.86 <sup>bc</sup>	Ca XIX	7.79 <sup>b</sup>	Ni XXVII		
2.51 <sup>b</sup>	Si XIV	3.90 <sup>bc</sup>	Ca XIX	7.81 <sup>b</sup>	Fe XXV		
2.62 <sup>b</sup>	Si XIV	3.93 <sup>bc</sup>	Ar XVIII	7.88 <sup>b</sup>	Fe XXV		
2.88 <sup>b</sup>	Si XV	4.10 <sup>bc</sup>	Ca XX	8.29 <sup>b</sup>	Fe XXV		
3.12 <sup>bc</sup>	Ar XVII	4.58 <sup>bc</sup>	Ca XIX	8.30 <sup>b</sup>	Fe XXVI		
3.31 <sup>bc</sup>	Ar XVIII	5.69 <sup>bc</sup>	Cr XXIII	8.70 <sup>b</sup>	Fe XXVI		

<sup>b</sup> Remain in broad range model

<sup>c</sup> Remain in narrow range model

TABLE II. Known emission lines included in the model

with same local density and scale radius as above, the total mass within the field of view becomes  $M_{\text{fov}} = 2.5 \times 10^6 M_\odot$  with a weighted average distance of  $D_{\text{avg}} = 9.1 \text{ kpc}$  and for density squared we get  $8.5 \times 10^{15} M_\odot^2 \text{ kpc}^{-3}$  at 8 kpc. For decaying dark matter, the ratios of  $M_{\text{fov}}/D_{\text{avg}}^2$  differ by less than one per mille for the two profiles while it is more significant for the density squared.

decays, the probability is proportional to density while for annihilation like processes the interaction requires two particles and the probability is proportional to density squared. This includes scattering processes.

#### A. Decay like dark matter

In Fig. 3 (left) we present the general flux constraints on line emission and non-astrophysical line emission near Sgr A\*. These constraints apply to all dark matter candidates with mono-energetic photon emission proportional to the density whether from decay or other processes. For

The allowed decay rate leading to photon emission is shown in Fig. 3 (right) for one photon per decay. For two-photon interactions, the constraints are a factor of two stronger. Similarly for particles of Majorana type where the particles are their own anti-particles, the interaction probability doubles and the constraints are strengthened by a factor of two.

## V. GENERAL CONSTRAINTS

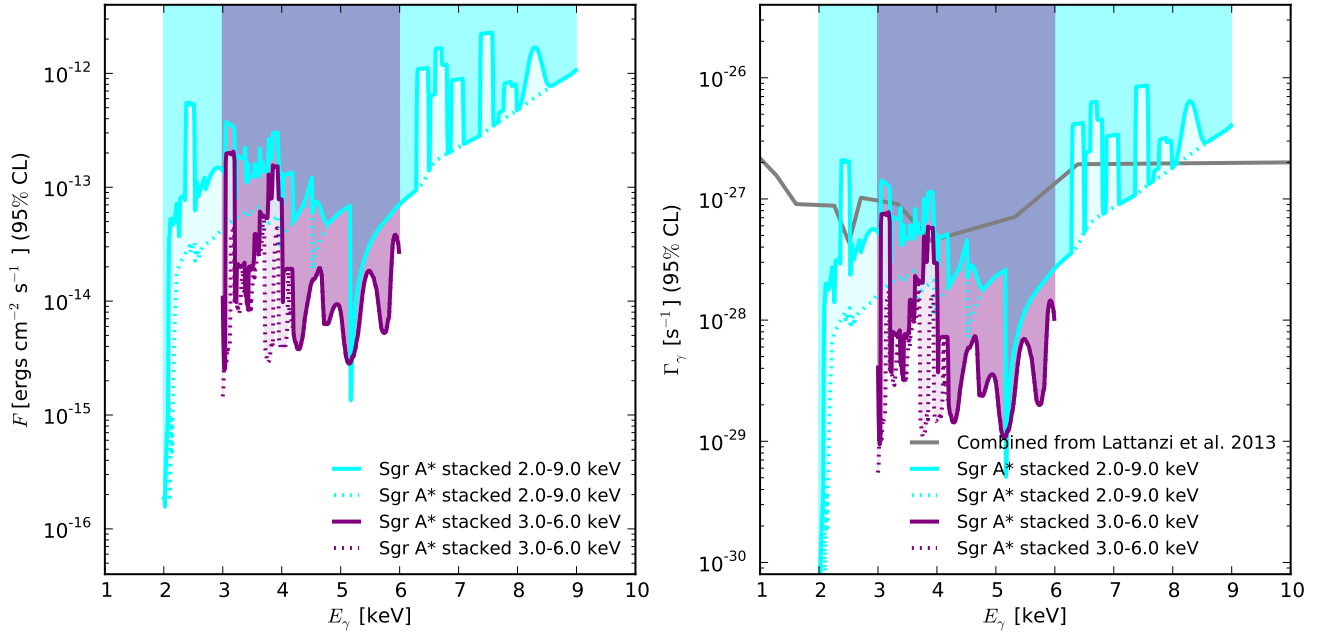


FIG. 3. **Left:** Constraints on line emission flux in the stacked spectrum (95% confidence). The cyan lines are for the entire 2-9 keV interval model, and the purple lines are for the 3-6 keV interval. The solid lines represent the total flux in line emission (including astrophysical lines) while for the dotted lines we have also subtracted the astrophysical lines in Tab. II. **Right:** General constraints on the interaction rate with one-photon emission proportional to matter density (95% confidence). The grey lines show the combination of previous constraints [12, and references therein] (same colours as for the left plot).

## B. Annihilation like dark matter

For annihilating dark matter, the local flux is given by

$$\begin{aligned} F_{\text{obs}} &= \frac{L_\gamma}{4\pi D_L^2} \\ &= \frac{1}{4\pi D_L^2} \frac{N_\gamma E_\gamma}{2m^2} \int \sigma v(r) \rho^2(r) dV, \end{aligned} \quad (4)$$

where  $m$  is the particle mass,  $N_\gamma$  is the number of photons per interaction,  $E_\gamma$  is the photon energy,  $\sigma$  is the interaction cross section,  $v(r)$  is the velocity distribution of the dark matter as a function of radius and the integral is over the observed volume. For a back-of-the-envelope calculation we assume two photons with  $E_\gamma = m/2$  per annihilation and that  $\langle \sigma v \rangle$  is independent of radius. Reordering and converting units we get

$$\begin{aligned} \langle \sigma v \rangle [\text{cm}^{-3} \text{sec}^{-1}] &= \\ &1.74 \times 10^{-11} \text{ cm}^{-3} \text{ sec}^{-1} F_{\text{obs}} [\text{erg cm}^{-2} \text{ sec}^{-1}] \\ &\times \frac{D_L^2 [\text{kpc}^2]}{\int \rho^2(r) dV [M_\odot^2 \text{ kpc}^{-3}]} \frac{m^2 [\text{keV}^2]}{E_\gamma [\text{keV}]} . \end{aligned} \quad (5)$$

The resulting constraint is plotted in Fig. 4.

## VI. CONSTRAINTS ON STERILE NEUTRINOS

The sterile neutrino is a strong particle candidate for dark matter viable with or without Super Symmetry

or Universal Extra Dimensions. With just three sterile neutrinos (gauge singlets), one can obtain the correct abundance of dark matter, a very simple explanation for the observed flavour oscillations and mass splittings of the active neutrinos, and a natural explanation for the baryon asymmetry [16–22]. The underlying particle model, called the  $\nu$ MSM, is described in detail in a number of papers [20, 21, 23–28], and recent reviews [29–31]. Additionally, the sterile neutrino may have interesting effects on a range of astrophysical objects, e. g. as an explanation for pulsar kick velocities, facilitating core collapse supernova explosions, affecting early star formation, reionization and structure formation, or assisting inflation [24, 32–43]. The lightest of the three sterile neutrinos provides a perfect dark matter candidate. The two free parameters of mass,  $m_s$ , and mixing angle with the active neutrinos,  $\sin^2(2\theta)$ , are unconstrained from particle physics, but various observations have already excluded large parts of this parameter space (see Fig. 5).

The mass is firmly bound from below through the phase space density of nearby dwarf galaxies. The Tremaine-Gunn bound [44] gives a model independent boundary of roughly 0.4 keV [45]. This limit can be increased if the production method is known, and e. g. for the resonant production the boundary is approximately 1 keV [45].

Observations of small scale structure from e. g. the Lyman  $\alpha$  forest can provide limits on the mass if the velocity distribution is known [46–49]. The velocity distribu-

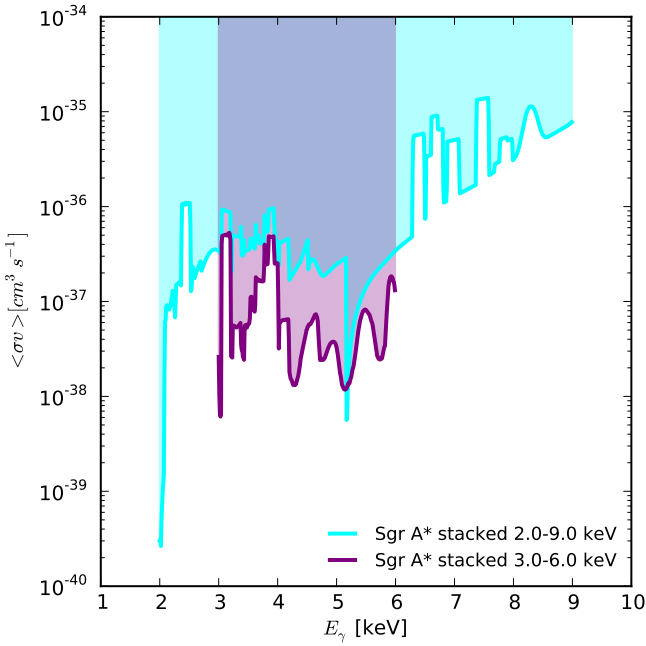


FIG. 4. Constraints on the velocity averaged cross-section for models with two-photon emission from dark matter annihilating into two photons from the total line emission flux.

tion of the sterile neutrinos depends on their production mechanism in the early Universe, and while the originally proposed non-resonant production [16] is ruled out, in general masses above  $m_s = 2$  keV are allowed [50]. An alternative mechanism is a resonant production [17], which requires a large initial lepton asymmetry [18, 51]. However, the lepton asymmetry cannot be so large that it violates Big Bang Nucleosynthesis, and consequently there is a strong lower limit on the mixing angle to produce enough sterile neutrinos to account for the observed dark matter density [26]. The sterile neutrinos can also be produced at the electro-weak scale by decays of a gauge singlet Higgs boson [30], or from their couplings to e. g. the inflaton [24].

The sterile neutrinos can decay via a one-loop diagram to an active neutrino and a photon. Since the two-body decay takes place almost at rest ( $v/c \approx 10^{-3}$  for galaxies), the decay line is very narrow and easily searched for in X-ray and soft gamma-ray observations. The fluxes are converted to constraints in the  $m_s - \sin^2(2\theta)$  parameter space for sterile neutrinos of the Majorana type, assuming the sterile neutrinos to account for all of the dark matter in the observed field of view [52, 53]:

$$\sin^2(2\theta) \leq 10^{18} \left( \frac{F_{\text{obs}}}{\text{erg cm}^{-2} \text{ sec}^{-1}} \right) \left( \frac{m_s}{\text{keV}} \right) \left[ \frac{(M_{\text{fov}}/\text{M}_\odot)}{(D_L/\text{Mpc})^2} \right] \quad (6)$$

where  $F_{\text{obs}}$  is the observed flux limit,  $M_{\text{fov}}$  is the total dark matter mass within the field of view, and  $D_{L,i}$  is the luminosity distance.

The 0.3–12 keV range is constrained from various objects observed with the *Chandra* and *XMM-Newton* X-ray telescopes [45, 52–62]. In Fig. 5 we show the strongest robust constraints from *XMM-Newton* observations of the Milky Way and M31 [58] and from *Chandra* observations of the Draco dwarf galaxy [59]. Some analyses have claimed stronger constraints, but were later found to be too optimistic [45, 55, 56, 58, 63–66]. The higher energy range of 3 – 48 keV has been constrained from the diffuse X-ray background observed with HEAO [54]. These constraints only depend on the amount and current properties of observed dark matter and are thus independent of the production mechanism.

Even the most conservative of the new constraints presented here do improve on previous constraints, and for the narrow interval the improvement is up to two orders of magnitude in flux. The green circle represents the inferred mass and mixing angle from Bulbul *et al.* [1] and the green shaded region is the Boyarsky *et al.* [2] result. Both results are allowed by the broad interval analysis when including all line emission flux but excluded at 95% confidence for the narrow interval analysis.

## VII. CONCLUSIONS

The Milky Way data does not clearly show the emission line detected in galaxy cluster spectra. The constraints on the allowed X-ray line emission flux are sensitive to the modelling of astrophysical emission lines but even in the most conservative case, they improve on previous constraints by up to two orders of magnitude. If one consider the narrow 3 – 6 keV interval sufficient for modelling the continuum flux around Sgr A\* (similar to the one used for clusters in Bulbul *et al.* [1]), the cluster signal is ruled out for decaying dark matter like sterile neutrinos

## ACKNOWLEDGMENTS

Thanks to Steen H. Hansen, Yassaman Farzan and Neal Weiner for inspiring discussions. SRS would like to thank NORDITA for hosting the News in Neutrino Physics 2014 workshop during which most of the analysis was carried out.

[1] E. Bulbul, M. Markevitch, A. Foster, R. K. Smith, M. Loewenstein, and S. W. Randall, ArXiv e-prints

(2014), arXiv:1402.2301 [astro-ph.CO].

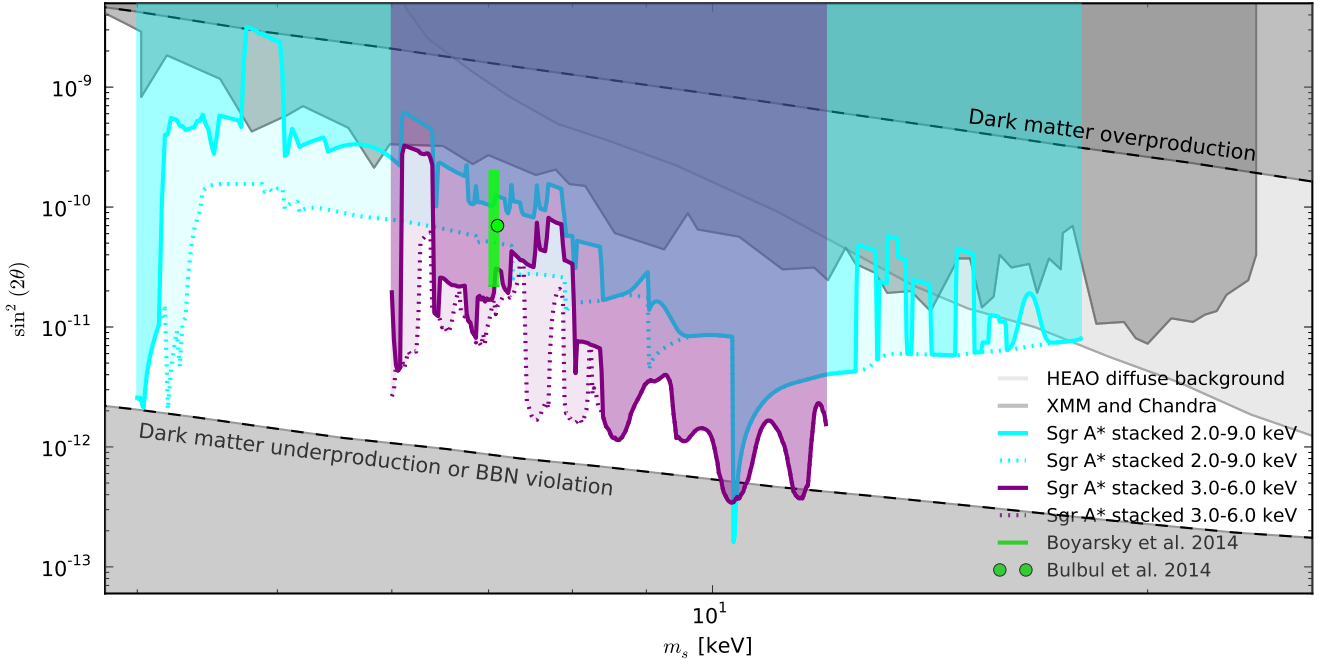


FIG. 5. Mass-mixing angle constraints on sterile neutrino like dark matter candidates. Above/below the dashed black lines the sterile neutrinos will be over/under produced relative to the observed dark matter density [22, 26]. The grey shaded regions are X-ray exclusion lines from *XMM-Newton* and *Chandra* observations [54, 58, 59], with the first rescaled by a factor of two due to mass estimate uncertainties as recommended in Boyarsky *et al.* [29]] and the coloured regions is the parameter space ruled out by the results presented here. The cyan lines are for the case where the entire 2-9 keV interval is modelled, and the purple lines are for the 3-6 keV interval. The solid lines are the total flux in line emission (including astrophysical lines) and for the dotted lines both the continuum and the astrophysical lines in Tab. II have been excluded.

- [2] A. Boyarsky, O. Ruchayskiy, D. Iakubovskyi, and J. Franse, ArXiv e-prints (2014), arXiv:1402.4119 [astro-ph.CO].
- [3] D. P. Finkbeiner and N. Weiner, (2014), arXiv:1402.6671 [hep-ph].
- [4] J. M. Cline, Y. Farzan, Z. Liu, G. D. Moore, and W. Xue, ArXiv e-prints (2014), arXiv:1404.3729 [hep-ph].
- [5] K. N. Abazajian, Physical Review Letters **112**, 161303 (2014), arXiv:1403.0954.
- [6] H. Ishida, K. S. Jeong, and F. Takahashi, Physics Letters B **732**, 196 (2014), arXiv:1402.5837 [hep-ph].
- [7] S. Chakraborty, D. K. Ghosh, and S. Roy, ArXiv e-prints (2014), arXiv:1405.6967 [hep-ph].
- [8] F. Bezrukov and D. Gorbunov, ArXiv e-prints (2014), arXiv:1403.4638 [hep-ph].
- [9] M. Revnivtsev, A. Vikhlinin, and S. Sazonov, Astronomy & Astrophysics **473**, 857 (2007), astro-ph/0611952.
- [10] R. K. Smith, N. S. Brickhouse, D. A. Liedahl, and J. C. Raymond, Astrophys. J. Lett. **556**, L91 (2001), astro-ph/0106478.
- [11] C. X. ray Center Chandra X-ray Center Chandra X-ray Center, Proposer's Observatory Guide **16** (2013).
- [12] M. Lattanzi, S. Riemer-Sørensen, M. Tórtola, and J. W. F. Valle, Phys. Rev. D **88**, 063528 (2013), arXiv:1303.4685 [astro-ph.HE].
- [13] J. Einasto and U. Haud, Astronomy & Astrophysics **223**, 89 (1989).
- [14] N. Bernal and S. Palomares-Ruiz, Journal of Cosmology and Astroparticle Physics **1**, 006 (2012), arXiv:1103.2377 [astro-ph.HE].
- [15] J. F. Navarro, C. S. Frenk, and S. D. M. White, Astrophys. J. **490**, 493 (1997), astro-ph/9611107.
- [16] S. Dodelson and L. M. Widrow, Physical Review Letters **72**, 17 (1994), arXiv:hep-ph/9303287.
- [17] X. Shi and G. M. Fuller, Physical Review Letters **82**, 2832 (1999), arXiv:astro-ph/9810076.
- [18] A. D. Dolgov and S. H. Hansen, Astroparticle Physics **16**, 339 (2002), arXiv:hep-ph/0009083.
- [19] K. Abazajian, G. M. Fuller, and M. Patel, Phys. Rev. D **64**, 023501 (2001), arXiv:astro-ph/0101524.
- [20] T. Asaka, S. Blanchet, and M. Shaposhnikov, Physics Letters B **631**, 151 (2005), arXiv:hep-ph/0503065.
- [21] T. Asaka and M. Shaposhnikov, Physics Letters B **620**, 17 (2005), arXiv:hep-ph/0505013.
- [22] L. Canetti, M. Drewes, and M. Shaposhnikov, Physical Review Letters **110**, 061801 (2013), arXiv:1204.3902 [hep-ph].
- [23] T. Asaka, M. Shaposhnikov, and M. Laine, JHEP **1**, 91 (2007), arXiv:hep-ph/0612182.
- [24] M. Shaposhnikov and I. Tkachev, Physics Letters B **639**, 414 (2006), arXiv:hep-ph/0604236.
- [25] D. Gorbunov and M. Shaposhnikov, JHEP **10**, 15 (2007), arXiv:0705.1729.
- [26] M. Laine and M. Shaposhnikov, Journal of Cosmology and Astro-Particle Physics **6**, 31 (2008), arXiv:0804.4543.
- [27] M. Shaposhnikov, JHEP **8**, 8 (2008), arXiv:0804.4542.
- [28] L. Canetti, M. Drewes, T. Frossard, and M. Shaposhnikov, ArXiv e-prints (2012), arXiv:1208.4607 [hep-ph].

- [29] A. Boyarsky, O. Ruchayskiy, and M. Shaposhnikov, Annual Review of Nuclear and Particle Science **59**, 191 (2009), arXiv:0901.0011 [hep-ph].
- [30] A. Kusenko, arXiv:0906.2968 (2009), arXiv:0906.2968.
- [31] M. Drewes, ArXiv:1303.6912 (2013).
- [32] A. Kusenko and G. Segrè, Physics Letters B **396**, 197 (1997), arXiv:hep-ph/9701311.
- [33] S. H. Hansen and Z. Haiman, Astrophys. J. **600**, 26 (2004), arXiv:astro-ph/0305126.
- [34] C. L. Fryer and A. Kusenko, Astrophys. J. Suppl. **163**, 335 (2006), arXiv:astro-ph/0512033.
- [35] J. Hidaka and G. M. Fuller, Phys. Rev. D **74**, 125015 (2006), arXiv:astro-ph/0609425.
- [36] P. L. Biermann and A. Kusenko, Physical Review Letters **96**, 091301 (2006), arXiv:astro-ph/0601004.
- [37] M. Mapelli, A. Ferrara, and E. Pierpaoli, Mon. Not. R. Astron. Soc. **369**, 1719 (2006), arXiv:astro-ph/0603237.
- [38] F. Bezrukov and M. Shaposhnikov, Physics Letters B **659**, 703 (2008), arXiv:0710.3755.
- [39] A. Kusenko, B. P. Mandal, and A. Mukherjee, Phys. Rev. D **77**, 123009 (2008), arXiv:0801.4734.
- [40] K. Petraki and A. Kusenko, Phys. Rev. D **77**, 065014 (2008), arXiv:0711.4646.
- [41] K. Petraki, Phys. Rev. D **77**, 105004 (2008), arXiv:0801.3470.
- [42] D. Boyanovsky, Phys. Rev. D **78**, 103505 (2008), arXiv:0807.0646.
- [43] D. Gorbunov, A. Khmelnitsky, and V. Rubakov, Journal of Cosmology and Astro-Particle Physics **10**, 41 (2008), arXiv:0808.3910.
- [44] S. Tremaine and J. E. Gunn, Physical Review Letters **42**, 407 (1979).
- [45] A. Boyarsky, D. Malyshev, A. Neronov, and O. Ruchayskiy, Mon. Not. R. Astron. Soc. **387**, 1345 (2008), arXiv:0710.4922.
- [46] S. H. Hansen, J. Lesgourgues, S. Pastor, and J. Silk, Mon. Not. R. Astron. Soc. **333**, 544 (2002), arXiv:astro-ph/0106108.
- [47] M. Viel, J. Lesgourgues, M. G. Haehnelt, S. Matarrese, and A. Riotto, Phys. Rev. D **71**, 063534 (2005), arXiv:astro-ph/0501562.
- [48] M. Viel, J. Lesgourgues, M. G. Haehnelt, S. Matarrese, and A. Riotto, Physical Review Letters **97**, 071301 (2006), arXiv:astro-ph/0605706.
- [49] U. Seljak, A. Makarov, P. McDonald, and H. Trac, Physical Review Letters **97**, 191303 (2006), arXiv:astro-ph/0602430.
- [50] A. Boyarsky, J. Lesgourgues, O. Ruchayskiy, and M. Viel, Physical Review Letters **102**, 201304 (2009), arXiv:0812.3256.
- [51] P. D. Serpico and G. G. Raffelt, Phys. Rev. D **71**, 127301 (2005), arXiv:astro-ph/0506162.
- [52] S. Riemer-Sørensen, S. H. Hansen, and K. Pedersen, Astrophys. J. Lett. **644**, L33 (2006), arXiv:astro-ph/0603661.
- [53] A. Boyarsky, J. Nevalainen, and O. Ruchayskiy, Astronomy & Astrophysics **471**, 51 (2007), arXiv:astro-ph/0610961.
- [54] A. Boyarsky, A. Neronov, O. Ruchayskiy, and M. Shaposhnikov, Mon. Not. R. Astron. Soc. **370**, 213 (2006), arXiv:astro-ph/0512509.
- [55] A. Boyarsky, A. Neronov, O. Ruchayskiy, M. Shaposhnikov, and I. Tkachev, Physical Review Letters **97**, 261302 (2006), arXiv:astro-ph/0603660.
- [56] K. Abazajian and S. M. Koushiappas, Phys. Rev. D **74**, 023527 (2006), arXiv:astro-ph/0605271.
- [57] S. Riemer-Sørensen, K. Pedersen, S. H. Hansen, and H. Dahle, Phys. Rev. D **76**, 043524 (2007), arXiv:astro-ph/0610034.
- [58] A. Boyarsky, D. Iakubovskyi, O. Ruchayskiy, and V. Savchenko, Mon. Not. R. Astron. Soc. **387**, 1361 (2008), arXiv:0709.2301.
- [59] S. Riemer-Sørensen and S. H. Hansen, ArXiv e-prints (2009), arXiv:0901.2569 [astro-ph.CO].
- [60] M. Loewenstein, A. Kusenko, and P. L. Biermann, Astrophys. J. **700**, 426 (2009), arXiv:0812.2710.
- [61] M. Loewenstein and A. Kusenko, Astrophys. J. **714**, 652 (2010), arXiv:0912.0552 [astro-ph.HE].
- [62] M. Loewenstein and A. Kusenko, Astrophys. J. **751**, 82 (2012), arXiv:1203.5229 [astro-ph.CO].
- [63] K. Abazajian, G. M. Fuller, and W. H. Tucker, Astrophys. J. **562**, 593 (2001), arXiv:astro-ph/0106002.
- [64] C. R. Watson, J. F. Beacom, H. Yüksel, and T. P. Walker, Phys. Rev. D **74**, 033009 (2006), arXiv:astro-ph/0605424.
- [65] H. Yüksel, J. F. Beacom, and C. R. Watson, Physical Review Letters **101**, 121301 (2008), arXiv:0706.4084.
- [66] C. R. Watson, Z. Li, and N. K. Polley, Journal of Cosmology and Astroparticle Physics **3**, 018 (2012), arXiv:1111.4217 [astro-ph.CO].